

Effectiveness of Turbulent Fountains in Frost Mitigation and Pollution Control

Daniel Freire Caporale,¹ Luis G. Sarasúa,¹ Nicasio Barrere,² and Arturo C. Martí¹

¹*Instituto de Física, Universidad de la República, Uruguay.*

²*Centro Universitario del Este, Universidad de la República, Uruguay.*

(*Electronic mail: dfreire@fisica.edu.uy)

(Dated: 30 September 2024)

We investigate the efficacy of turbulent fountains as a tool for frost mitigation and pollution control in stratified ambient fluids. By examining the interaction between the ejected fountain fluid and the lower atmospheric layers, we develop predictive models to assess their impact on temperature distribution and the return of polluted ejected fluid to the ground. This analysis covers a range of fountain parameters, including Fr^{-2} and u'/U , where Fr is the Froude number and u'/U represents the turbulent intensity at the inlet. Notably, we identify an optimal set of parameter values where the temperature rise is maximised, independent of the fountain's turbulence intensity. This optimal condition occurs in the so-called semi-collapse regime, as described by Sarasúa et al. [Flow, Turbulence and Combustion, 112(4), 1009-1025 (2024)], where the returning fluid, mixed with warmer upper ambient layers, significantly increases local temperature. Our findings underscore the importance of carefully tuning fountain parameters to balance their effects on the surrounding environment, offering valuable insights for the practical use of turbulent fountains in environmental management.

I. INTRODUCTION

A fountain, defined as a vertical buoyant jet where the buoyancy force opposes the jet's initial velocity, contrasts with a plume, in which buoyancy and velocity are aligned. Both fountains and plumes are ubiquitous in natural systems and technological applications, particularly where the dynamics of stratified fluids are of interest. Research into turbulent fountains and plumes in both homogeneous and stratified environments has spanned several decades (e.g., Morton et al. 1956¹; Kaye 2008²; Woods 2010³), with early studies focusing on turbulent jets due to their relevance in atmospheric science and environmental engineering.

Fountain dynamics in stratified media exhibit several key features. As the fountain rises, it decelerates due to the combined effects of ambient fluid entrainment and opposing buoyancy, eventually reaching a maximum height, h_m , where the vertical momentum vanishes. The fluid then reverses direction, descending as an annular plume and spreading outward to form a "spreading cloud" at a height h_{sp} above the fountain ($h_{sp} > 0$), or collapsing back to the ground ($h_{sp} \simeq 0$)⁴. This spreading or collapse depends strongly on the initial momentum, buoyancy flux, and the stratification profile of the surrounding medium. In Fig. 1, we show a schematic of the flow in a no-collapse scenario, highlighting the characteristic flow heights. Additionally, the minimal height, h_c , defined as the minimum height of the lower boundary of the spreading cloud and introduced in Sarasúa et al. (2024)⁴, is also indicated. In orange, we outline the path of the fountain fluid, from injection to radial movement within the spreading cloud, where the fluid moves away from the fountain axis at height h_{sp} . In blue, the entrainment of ambient fluid by the fountain is shown, and in red, the movement of displaced ambient fluid during the formation and stabilisation of the spreading cloud is indicated.

As a practical application of fountain dynamics, we refer

an innovative technology aimed at protecting crops from frost damage, operating under conditions where no collapse occurs. Frost control in agriculture is critically important, as crop damage depends on both temperature and the duration of exposure, with severe damage occurring at temperatures below -2 °C^{5,6}. During radiation frost events, the Earth's surface cools predominantly due to radiative heat loss, leading to the formation of a temperature inversion where the air near the ground becomes the densest and coolest within the ambient environment. This creates an atmospheric stratification characterised by a linear temperature profile with height, as illustrated in Fig. 2. An effective technological solution to this problem is the Selective Inverted Sink (SIS)⁷ (Guarga et al. 2000⁸). The SIS works by ejecting cold air upwards, displacing the densest layer of cold air near the ground. This process also entrains air from the surrounding atmosphere (Albertson et al. 1950⁹).

A better understanding of these fountain dynamics could further enhance frost protection strategies in agriculture (Arias et al. 2007¹⁰; Yazdanpanah and Stigter 2011¹¹; Vahid et al. 2015¹²; Hu et al. 2018¹³). Figure 2 illustrates the core mechanism of the SIS: a vertical-axis propeller draws cold, dense air from the surface through an inlet and expels it upwards through the outlet. Since the SIS operates under conditions that prevent fountain collapse, the cold air does not return to the surface. This upward removal of cold air allows warmer air layers above to descend, thus preventing harmful temperatures near the surface that could damage crops. Following this approach, further applications of the SIS have been proposed for controlling contaminants such as odours or dust in open-pit mining environments¹⁴.

The seminal work by Morton et al. (1956)¹ introduced the foundational *MTT* model, which describes the evolution of volume, momentum, and buoyancy fluxes in fountains. While this model effectively predicts the maximum height in uniform ambient fluids, it does not fully capture post-reversal dynamics or spreading behaviour in stratified environments.

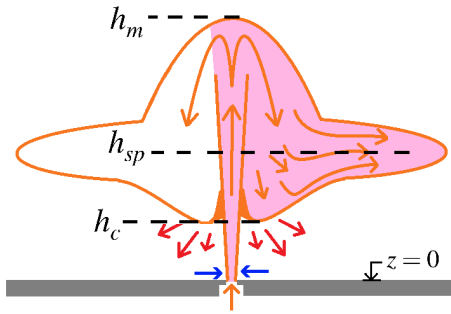


FIG. 1: Two-dimensional schematic of the fountain flow and the characteristic heights of its dynamics in the developed flow regime: the maximum height (h_m) attained by the fountain, the spreading height (h_{sp}), around which the fountain spreads radially away from the axis in the form of a “spreading cloud”, and the minimal height (h_c), defining the lower boundary of the spreading cloud. The region occupied by the fountain is highlighted in purple, representing fluid either injected or entrained from the surrounding ambient. Arrows indicate the motion of fluid: orange arrows represent fluid from the fountain, blue arrows correspond to the entrainment of ambient fluid near the fountain’s inlet and red arrows, below the h_c level, depict the movement of ambient fluid displaced downward during the formation of the spreading cloud.

Bloomfield and Kerr (1998)¹⁵ sought to address these limitations by relating the spreading height to the point where fluid densities match. However, their model overlooked the important role of mixing between the fountain and ambient fluid during the downflow phase.

Subsequent studies, such as those by Kaminski et al. (2005)¹⁶, refined the understanding of turbulent entrainment by introducing experimentally determined entrainment coefficients, while Mehaddi et al. (2011)¹⁷ examined maximum heights in stratified environments. Papanicolaou and Stamoulis (2010)¹⁸ further explored collapse and spreading phenomena. Several studies (e.g., van Reeuwijk and Craske 2015¹⁹) emphasised the variability of the entrainment coefficient with turbulence intensity, a crucial factor in fountain behaviour. Recent advances include the work of Sarasúa et al. (2021)²¹, who extended the *MTT* framework by incorporating additional parameters, such as the turbulent entrainment coefficient and buoyancy frequency, to more accurately predict collapse and spreading behaviour in axisymmetric turbulent fountains. Freire Caporale et al. (2022)²² further advanced the field by examining Lagrangian coherent structures in the downflow region, using finite-time Lyapunov exponents to quantify entrainment and re-entrainment, thereby improving the understanding of the mechanisms governing fountain dynamics. Freire et al. (2010)²³ previously investigated the influence of fluctuations on fountain heights h_m and h_{sp} , while Sarasúa et al. (2024)⁴ developed a diagram summarising these dependencies, providing practical insights for industrial applications of turbulent fountains. The latter study focused on the collapse of turbulent fountains, analysing the impact of turbulence intensity and the Froude number, two key param-

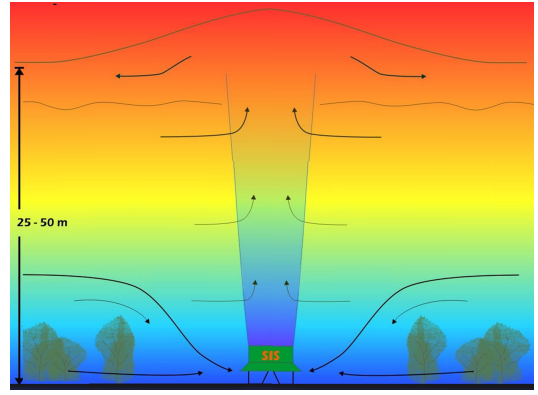


FIG. 2: SIS operation under radiation frost conditions. The linear temperature stratification of the atmosphere is represented by a colour gradient from blue (cold) to red (warm). In a typical operation scenario, h_{sp} ranges from 25 to 50 m. (Illustration adapted with permission from Frost Protection Co. from its website²⁰.)

eters regulating fountain dynamics. These authors identified three distinct regimes based on h_{sp} and h_c , indicated in Fig. 1: the collapse regime, where $h_{sp} = 0$; the semi-collapse regime, where $h_{sp} > 0$ and $h_c = 0$; and the no-collapse regime, where both $h_{sp} > 0$ and $h_c > 0$. Based on this analysis, the authors developed a diagram that divides the configuration space of the fountain (turbulence intensity and Froude number) into regions where each flow regime occurs.

In this work, we focus on analysing the effect of the fountain flow on the surrounding ambient fluid. While Sarasúa et al. (2024)⁴ investigate the characteristics and flow regime of the fountain based on inlet conditions, the impact on the ambient fluid is not addressed. In this study, we concentrate on that aspect, examining the evolution of the temperature in the lower layers of the ambient fluid (where the SIS operates to increase it and thus protect crops), as well as the concentration of ejected fountain fluid that returns to the ground and the radial distance from the fountain axis where this returning fluid is detected. If we consider that the ejected fluid contains contaminants, it becomes crucial to determine whether it has been entirely removed or what proportion still remains detectable at ground level. Understanding the impact of the fountain flow on the surrounding environment provides a significant contribution to the technological potential of turbulent fountains, aiding in the identification of optimal application conditions.

The paper is organised as follows. In Sec. II, we detail the methodology employed, which consists of computational simulations validated through laboratory experiments previously^{21,22} conducted. Then, in Sec. III, we present the results along with their analysis, focusing on the impact of the fountain’s flow on the temperature of the lower fluid layers and the return of ejected fluid, as a function of the fountain’s characteristics. Finally, in Sec. IV, we provide the conclusion and outline some potential directions for future work.

II. METHODOLOGY

In this work, the analysis was conducted based on computer simulations using the open-source Computational Fluid Dynamics (CFD) package `caffa3d.MBRi`²⁴, which implements a fully implicit second-order scheme in both time and space, supporting curvilinear meshes and following the Finite Volume Method (FVM)²⁵. The numerical results were validated against previously conducted laboratory experiments^{21,22}, whose setup was designed to rescale the operational conditions of the SIS. This rescaling was achieved through an analysis of the relevant non-dimensional numbers.

As in the laboratory-scale implementation of the SIS's real-world application, a prismatic computational domain measuring 40 cm × 40 cm × 50 cm in width (x), depth (y), and height (z) was employed. The working fluid for both the ambient and the fountain was water. The simulations used a time step of 0.05 s, and the domain was discretised with a computational mesh of 8×10^6 cells. Mesh independence was confirmed, as no significant differences were observed when using either a coarser mesh of 2×10^6 cells or a finer mesh of 30×10^6 cells.

The initial stratification of the ambient fluid follows a linear temperature profile, given by $T_0(z) = T(x, y, z, t = 0) = \partial_z T \cdot z + T_{cold}$, where $T_{cold} = 15 \text{ }^\circ\text{C}$ and $\partial_z T = 25 \text{ }^\circ\text{C} \cdot \text{m}^{-1}$, i.e., $T_{hot} = T(x, y, z = 50 \text{ cm}, t) = 27.5 \text{ }^\circ\text{C}$. Under these conditions, the corresponding characteristic Brünt-Väisälä frequency is $N = 0.232 \text{ s}^{-1}$. The fountain is injected vertically at temperature T_{jet} through a small circular nozzle with a diameter of $D = 0.8 \text{ cm}$, located at the centre of the base of the domain at $x = y = 0$. Calculations were repeated for $T_{jet} = 4.0, 6.0, 7.5, 10.0, 12.5$ and $15.0 \text{ }^\circ\text{C}$.

The boundary conditions of the domain are wall boundaries on all sides, except for the inlet condition at the centre of the base and the outlet condition through a small nozzle at the centre of the upper boundary, with a diameter of 4.0 cm, where a fully developed flow exit condition was applied. The boundary conditions for temperature are adiabatic on the lateral walls, with constant temperature at the lower boundary $T(x, y, z = 0, t) = T_{cold}$, and $T(x, y, z = 50 \text{ cm}, t) = T_{hot}$ on the upper boundary.

At each time step, the fluid velocity in the computational cells at the inlet is given by $\mathbf{U}^{\text{in}} = (u_x, u_y, u_z + U)$, where u_x , u_y , and u_z are randomly assigned within the interval $[-u', +u']$ at each time step, following a uniform distribution, and $U = q_{in}/\pi D^2$, where $q_{in} = 5.5 \text{ cm}^3 \cdot \text{s}^{-1}$ is the fountain's flowrate at the inlet. In this work, for each value of T_{jet} , calculations were repeated for different values of u' to vary the turbulence intensity u'/U , taking the values 0, 1, 2, 4, 10 and 20 %. Note that at each time step, $u_z + U$ is corrected by a multiplicative factor to ensure that the average over the computational cells at the fountain inlet equals U . The turbulence model used is the standard Smagorinsky large-eddy model, with a Smagorinsky coefficient for subgrid viscosity of $C_S = 0.16$ in our simulations. Due to the random nature of the imposed fluctuations, simulations were repeated under the same fountain configuration for several cases, yielding similar results.

In this work, we analyse the temperature field to study its evolution in the lower layers of the ambient fluid. Ad-

ditionally, to investigate the mixing phenomenon, a passive scalar field, represented by $\Phi(x, y, z, t)$, was used to track the concentration of injected fluid. Initially, $\Phi(x, y, z, t = 0) = 0$ throughout the domain, except in the cells located at the inlet nozzle, where $\Phi = 1$ at all times. Thus, advection, entrainment, mixing, and diffusion cause $\Phi(x, y, z, t)$ to take values between 0 and 1 throughout the domain, representing the concentration of fluid injected by the fountain. Figure. 3 shows a typical computationally obtained Φ field, represented in red shades, in a fully developed flow scenario for the configuration $T_{jet} = 15 \text{ }^\circ\text{C}$ and $u'/U = 20 \text{ }%$.

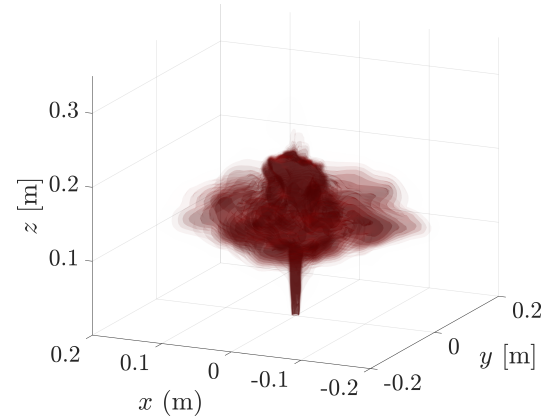


FIG. 3: Three-dimensional view of the passive scalar field Φ , represented in red shades, corresponding to values of Φ between 0 (white) and 1 (red). This case corresponds to a fountain temperature of $T_{jet} = 15 \text{ }^\circ\text{C}$ and a turbulence intensity of $u'/U = 20 \text{ }%$ at $t = 80 \text{ s}$, when the flow is fully developed.

The validation of the computational simulations was conducted by comparing the tracer fields with the previously performed experimental measurements^{21,22}. This was achieved by analysing both the shape of the fountain over time and the evolution of h_m and h_{sp} . As an example, Fig.4 compares a photograph of the tracer-marked fountain obtained experimentally for $T_{jet} = 15 \text{ }^\circ\text{C}$, using an 80-wire-per-inch mesh screen (with each wire having a diameter of 0.18mm) placed transversely at the inlet to generate a specific turbulence level, referred to as the “grid” configuration, with the corresponding simulation for $u'/U = 20 \text{ }%$, both at $t = 80 \text{ s}$. As can be seen, the overall shape of the fountain, as well as the heights it reaches, are in excellent agreement.

Additionally, Fig. 5 shows the evolution of h_m and h_{sp} for two experimental configurations: one referred to as “free”, where $T_{jet} = 15 \text{ }^\circ\text{C}$ and no mesh screen was placed at the inlet, and the other being the grid configuration. These experimental results are shown alongside the computational simulation results for turbulence intensities of $u'/U = 2$ and $20 \text{ }%$, respectively. The computational and experimental data for the two configurations, free and grid, exhibit excellent agreement, further confirming the accuracy of the numerical simulations. This robust correlation between the simulations and laboratory experiments underscores the ability of the numerical model to faithfully reproduce the essential dynamics of turbulent fountains.

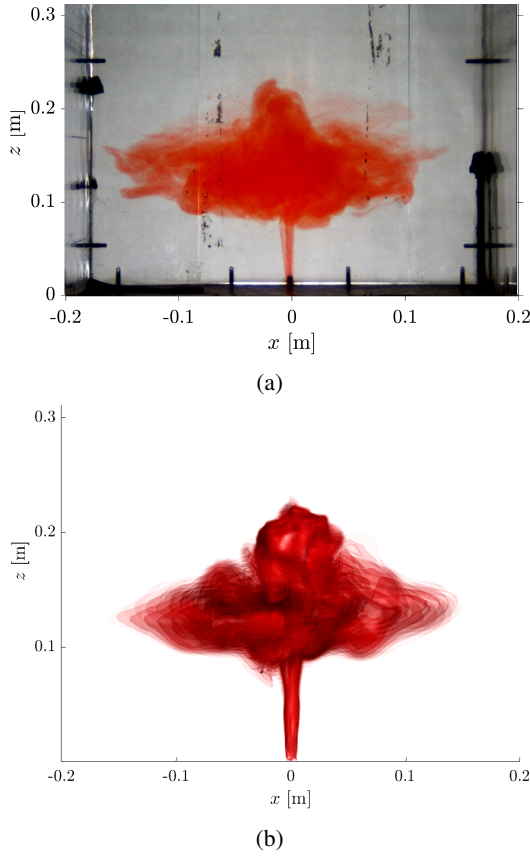


FIG. 4: Tracer fields of the fountain with fully developed flow at $t = 80$ s for: (a) experimental measurements with the grid configuration and (b) computational results for a turbulence intensity of $u'/U = 20\%$.

III. ANALYSIS AND RESULTS

In this work, we analyse the impact of turbulent fountains on the lower layers of the ambient fluid as a function of two key parameters influencing the flow⁴, namely the fountain characteristics, i.e., T_{jet} and u'/U . As in Sarasúa et al. (2024)⁴, we work in the configuration space $(Fr^{-2}, u'/U)$, where Fr represents the Froude number at the fountain inlet, which is defined as $Fr = U / \sqrt{gD \frac{\rho_{jet} - \rho_{00}}{\rho_{00}}}$, where D is the fountain inlet diameter, U is the mean inlet velocity, ρ_{jet} is the density of the fountain at the inlet, and ρ_{00} is the initial density of the stratified ambient fluid at $z = 0$. These densities correspond to those of water at the given temperatures.

The performance of fountains with different characteristics is assessed using the efficiency indicators we propose, tailored to their specific applications. Firstly, their ability to mitigate low ambient fluid temperatures near ground level is evaluated in Sec. III A. Secondly, in Sec. III B, we discuss the presence of a tracer as an indicator of the concentration of fluid that, after being ejected as a fountain, returns to the ground. Finally, in Sec. III C, the radial threshold distance is determined, measured from the fountain's point of emission, beyond which the

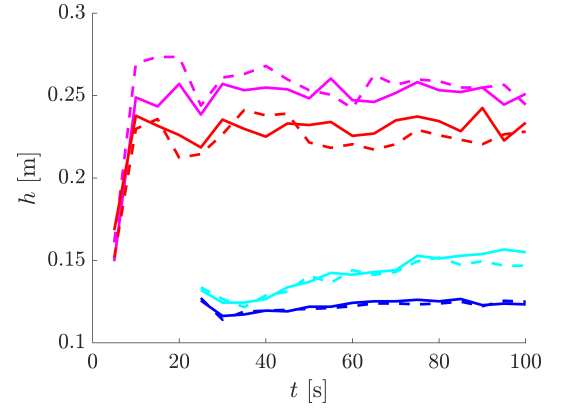


FIG. 5: Evolution of h_m and h_{sp} obtained from previously conducted laboratory experiments^{21,22} (solid lines) and computational simulations (dashed lines). In magenta (red), the evolution of h_m for the free (grid) experimental configuration is shown, corresponding to a turbulence intensity of $u'/U = 2\%$ ($u'/U = 20\%$) in the computational simulations. In cyan (blue), h_{sp} is shown for the free (grid) configuration. After $t \approx 70$ s, all heights stabilise, and the flow becomes fully developed, as shown in Fig. 4.

tracer concentration falls below a specified tolerance value.

A. Average temperature change in the lower layers

The phenomenon of entrainment (*MTT* model¹) causes the fountain to incorporate fluid from its surroundings during its ascent, depending on the relative velocity conditions between the fountain and the ambient fluid, as well as the turbulence level of the ejected flow²¹. There is a delicate interaction of different mechanisms -advection, diffusion, and mixing- that governs both the dynamics of the fountain and the evolution of the ambient fluid around it. Previous literature focuses on analysing the characteristic heights reached by the fountain, i.e., the maximum, spreading, and minimal heights, but the evolution of the ambient fluid, especially near ground level where fountain action may have technological significance, has not been thoroughly addressed⁸.

We analyse the increase in the average ambient temperature in areas surrounding the fountain, within different radial distances r from the centre of the fluid inlet, with $r \geq D$. For this purpose, we first calculate the azimuthal average of the temperature field $T(x, y, z, t)$ to smooth out fluctuations inherent to the flow and obtain a temperature field as a function of the vertical coordinate z and the radial distance from the fountain axis, r . Then, given the ambient fluid temperature at a point (r', z') at time t , $T(r', z', t)$, and the initial temperature at the same point, $T(r', z', t = 0) = T_0(z')$, we define the average temperature increase of the ambient fluid within the lower layers, below a specified height z , and at a radial distance less than r (but greater than D), at time t , as

$$\Delta T_{\text{avg}}(r, z, t) = \langle T(r', z', t) - T_0(z') \rangle_{(r', z') \in \mathcal{R}(r, z)} \quad (1)$$

where $\langle f \rangle_{\mathfrak{R}(r,z)}$ represents the spatial average of a scalar field f over the region $\mathfrak{R}(r,z)$, defined as

$$\mathfrak{R}(r,z) = \{(r',z'), \text{ such that } D \leq r' \leq r \text{ and } 0 \leq z' \leq z\} \quad (2)$$

Here, ΔT_{avg} is expressed in degrees Celsius ($^{\circ}\text{C}$), although it can equally be expressed in Kelvin (K), as it represents a temperature difference.

For this analysis, we first determine the moment from which the conditions in the lower layers of the ambient fluid stabilise. Here, we arbitrarily consider the lower layers of the ambient fluid as those located in $0 \leq z \leq 3D$. We then seek to determine the time τ such that the shape of the profile $\langle T(r,z,t) - T_0(z) \rangle_{0 \leq z \leq 3D}$ as a function of r stabilises for $t \geq \tau$. In Fig. 6, this profile is shown at different time instants for two arbitrarily chosen fountain configurations as a function of the non-dimensional radial distance $r^* = r/D$ (with $r^* = 25$ being the maximum radius of the domain). As observed, the profiles cease to vary (except for inherent turbulent flow fluctuations) and stabilise into a steady profile in the fully developed flow regime at $\tau = 125$ s. Although this analysis is presented here for two arbitrary configurations, this stabilisation time was explored for the other configurations considered in this work, and the same behaviour was consistently observed.

Based on the time at which the temperature increase profiles converge, we calculate the net ambient temperature rise, ΔT_{avg} , from Eq. 1, for the different computational configurations at time $t = 135$ s. In Fig. 7(a), we present a colour map of $\Delta T_{\text{avg}}(r = 5D, z = 3D, t = 135\text{s})$ in the configuration space $(Fr^{-2}, u'/U)$. Fig. 7(b) shows the corresponding data for $\Delta T_{\text{avg}}(r = 10D, z = 3D, t = 135\text{s})$. The general pattern of the two maps is similar, indicating that the average increase in ambient fluid temperature in the lower layers is largely independent of radial distance. The impact of the flow on the near-ground ambient is particularly noteworthy. Firstly, for $Fr^{-2} \leq 5 \times 10^{-3}$, i.e., fountain temperatures above approximately 4°C , there is always an increase in the average temperature of the lowest layers of the ambient fluid. The largest temperature increase is observed primarily in a region of the configuration space with $2.2 \times 10^{-3} \leq Fr^{-2} \leq 5.3 \times 10^{-3}$ (fountain temperatures in the range of approximately 4 – 12.5°C). However, this region is irregular in shape and narrows for turbulence intensities in the range $1\% \geq u'/U \geq 3\%$, covering the interval $3.8 \times 10^{-3} \leq Fr^{-2} \leq 5.3 \times 10^{-3}$ (fountain temperatures in the range of approximately 4 – 10°C).

This behaviour is noteworthy but can be explained by the fountain collapse diagram from Sarasúa et al. (2024)⁴, which outlines the regions of the configuration space $(Fr^{-2}, u'/U)$ corresponding to non-collapse, semi-collapse, and full collapse of the fountain. The collapse region, i.e., configurations where the spreading height is $h_{sp} = 0$, is indicated for $Fr^{-2} \geq 5.3 \times 10^{-3}$, regardless of turbulence intensity. In this region, a cooling of the lower layers of the ambient fluid is observed, as shown in Fig. 6. Given that, during fountain collapse, fluid with a high tracer concentration is detected at ground level, meaning it has undergone little mixing with the ambient fluid during its ascent, and that this mixing only occurs up to small maximum fountain heights (h_m), the tempera-

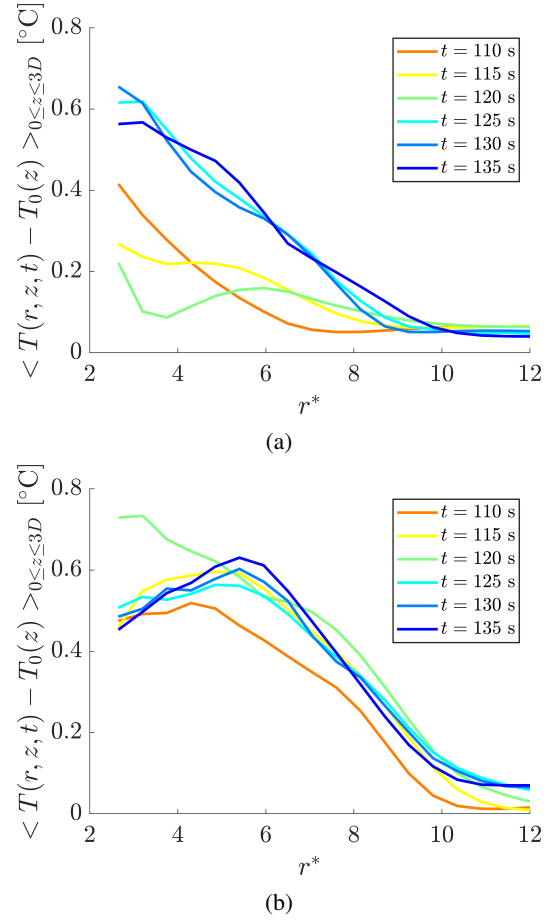


FIG. 6: Profiles of $\langle T(r,z,t) - T_0(z) \rangle_{0 \leq z \leq 3D}$ for different time instants as a function of r^* , for the fountain configurations: (a) $(Fr^{-2}, u'/U) = (3.8 \times 10^{-3}, 4\%)$, and (b) $(Fr^{-2}, u'/U) = (4.9 \times 10^{-3}, 2\%)$.

ture of the fountain fluid returning to the ground is low enough to cause the cooling of the lower ambient fluid layers.

On the other hand, for $Fr^{-2} \leq 5.3 \times 10^{-3}$, the collapse diagram separates the regions of non-collapse and semi-collapse, both characterised by $h_{sp} > 0$. To distinguish between these regimes, an arbitrary tracer concentration tolerance, Φ_{tol} , is introduced in Sarasúa et al. (2024)⁴. The non-collapse regime is defined as the set of configurations where, once the fully developed flow state is reached, $\Phi(x, y, z, t) < \Phi_{tol}$ across the entire ground level, i.e., $z = 0$, while the semi-collapse region corresponds to configurations where $\Phi > \Phi_{tol}$ at any point in the ambient fluid at ground level. It is important to note that, for constructing the collapse diagram in such work, Φ was considered within the ambient fluid layer near the ground, rather than averaged over the lower layers.

The region of the configuration space where the greatest heating of the lower layers of the ambient fluid is detected (see Fig 7) lies within the semi-collapse region of the collapse diagram, regardless of the value of Φ_{tol} considered. Therefore, the semi-collapse of the fountain promotes the average increase in temperature of the lower layers of the ambient

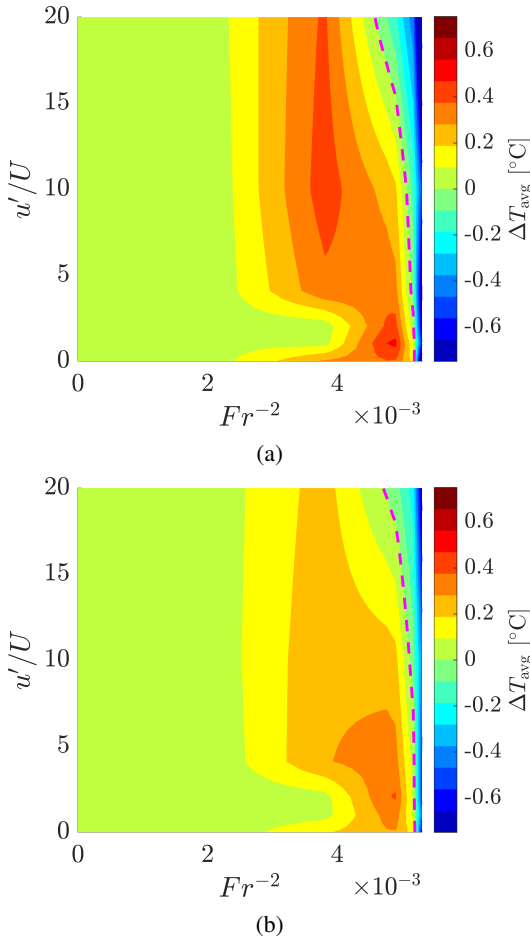


FIG. 7: Two-dimensional colour map of the mean temperature increase in the lower layers of the ambient fluid: (a) $\Delta T_{\text{avg}}(r = 5D, z = 3D, t = 135s)$, and (b) $\Delta T_{\text{avg}}(r = 10D, z = 3D, t = 135s)$. The magenta dashed line marks the right boundary of the configuration space where ΔT_{avg} is positive.

fluid. To better understand the underlying mechanism of this phenomenon, it is necessary to reference the minimal height, h_c , defined in Sarasúa et al. (2024)⁴ as the lower boundary of the spreading cloud (which is outlined by the tracer in the fully developed flow regime, where the ejected fountain fluid spreads radially, moving away from the fountain; see Fig. 1). In the configurations where heating of the lower layers of the ambient fluid is detected in Fig. 7, we observe that $h_c > 0$ and it increases as Fr^{-2} decreases. Thus, it is easy to envision how, during the transient stage of the flow and up until the fully developed flow regime, the spreading cloud displaces ambient fluid from higher layers, but below h_{sp} , downwards (such motion is represented with red arrows in Fig. 1). This fluid mixes with the lower layers of the ambient fluid, leading to more efficient heating of these layers.

Supporting this potential heating mechanism, the collapse diagram shows a narrowing of the semi-collapse region for lower turbulence intensities, which coincides with the narrowing of the region of greatest heating in the lower layers of the

ambient fluid, as explained by the results in Fig. 7. From this analysis, we observe that the evolution of the ambient fluid is strongly dependent on the characteristics of the flow induced by the fountain during the fully developed flow stages.

B. Return of ejected fluid: Tracer concentration in the lower layers

Let us assume, motivated by the applications of the SIS device introduced in Sec. I, that the fountain fluid, which is denser than the ambient fluid, represents a fluid containing some type of contaminant. It is crucial, therefore, to determine how much “contaminated” fluid, depending on the fountain configuration, comes back into contact with the ground. In this work, we perform a detailed analysis of the average tracer concentration in the lower layers of the ambient fluid within two radial distances from the fountain entry.

The proposed method first involves, similar to Sec. III A, obtaining the field $\phi(r, z, t)$, which represents the azimuthal average of the tracer field $\Phi(x, y, z, t)$ around the fountain axis, $r = 0$, at each time instant. Then, analogous to the procedure applied to $\Delta T_{\text{avg}}(r, z, t)$ in Eq. 1, we define the average tracer concentration over the lower layers of the ambient fluid at time t , $\phi_{\text{avg}}(r, z, t)$, as

$$\phi_{\text{avg}}(r, z, t) = \langle \phi(r', z', t) \rangle_{(r', z') \in \mathfrak{R}(r, z)} \quad (3)$$

where $\mathfrak{R}(r, z)$ is the region defined in Eq. 2.

To determine the moment τ from which the average tracer concentration in the lower layers of the ambient fluid stabilises, we study, similarly to what was done in Sec. III A, the evolution of the profile $\langle \phi(r, z, t) \rangle_{0 \leq z \leq 3D}$ at different time instants. Figure 8 shows such profiles for two arbitrarily selected fountain configurations. In all cases, we observe that for $t \geq 125$ s, the average tracer concentration ceases to evolve. Therefore, in this section, we choose the time $t = 135$ s, as we did with the average temperature increase in Sec. III A, to analyse the average tracer field.

Once the time instant for analysis is determined, in Fig. 9(a) we show the colour map of $\phi_{\text{avg}}(r = 5D, z = 3D, t = 135s)$, and Fig. 9(b) shows the corresponding map for $\phi_{\text{avg}}(r = 10D, z = 3D, t = 135s)$. The first observation from these figures is, as in Sec. III A, their strong similarity, indicating that when the fountain fluid comes into contact with the lower layers of the ambient fluid, the tracer distribution is relatively uniform in the radial direction for $r^* \leq 10$.

Secondly, by comparing Figures 7 and 9, we observe an overlap between the regions of temperature increase in the ambient fluid and the detection of the tracer in the lower layers. This overlap indicates that the presence of fountain fluid returning to the ground after mixing with the warmer, upper layers of ambient fluid contributes to the overall increase in the mean temperature of the lower layers.

Furthermore, let us consider a region in the configuration space where the temperature increase is most pronounced. As seen in Fig. 7, this occurs, for example, at $Fr^{-2} = 3.8 \times 10^{-3}$

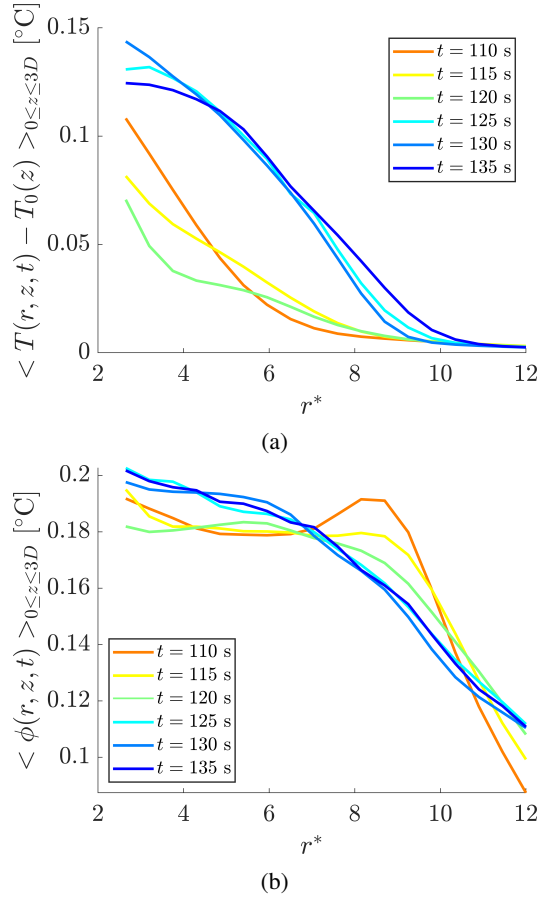


FIG. 8: Profiles of $\langle \phi(r, z, t) \rangle_{0 \leq z \leq 3D}$ as a function of r^* , for different time instants, and the configurations: (a) $(Fr^{-2}, u'/U) = (3.8 \times 10^{-3}, 4\%)$, and (b) $(Fr^{-2}, u'/U) = (4.9 \times 10^{-3}, 2\%)$.

and $u'/U > 6\%$. If we examine the average tracer concentration in the lower layers of the ambient fluid for the same region, as shown in Fig. 9, the values range between $0.10 < \phi_{\text{avg}} < 0.15$. This suggests a low concentration of fountain fluid, indicating that most of the fluid present is ambient fluid that was entrained and displaced from the upper layers of the environment. This finding reinforces the hypotheses presented in Sec. III A regarding the mechanisms that govern the conditions of the lower layers of the ambient fluid. As we move away from this configuration of maximum ambient heating, two scenarios arise: either we shift to configurations with lower Fr^{-2} (i.e., higher T_{jet}), where the fountain reaches greater heights and does not displace significant amounts of warmer ambient fluid downwards, or we shift to configurations with higher Fr^{-2} (i.e., lower T_{jet}), where the fountain reaches lower heights and tends to settle near the ground, with minimal mixing with the warmer upper layers of the ambient fluid, and thus without having significantly increased its temperature beforehand.

By identifying and supporting this correlation between the average tracer concentration and the average temperature increase in the lower layers of ambient fluid, we can explain the

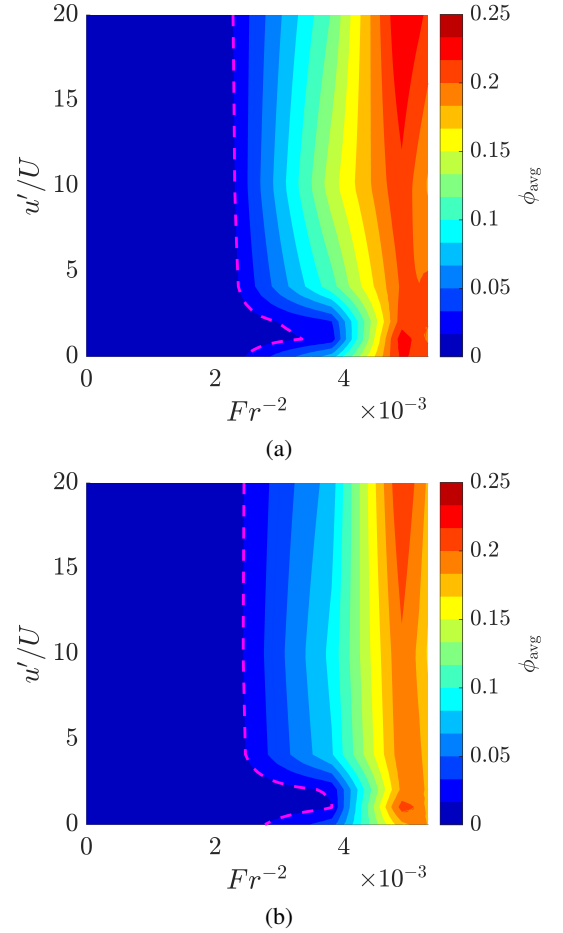


FIG. 9: Two-dimensional colour map of the mean tracer concentration in the lower layers of the ambient fluid: (a) $\phi_{\text{avg}}(r = 5D, z = 3D, t = 135\text{s})$, and (b) $\phi_{\text{avg}}(r = 10D, z = 3D, t = 135\text{s})$. The magenta dashed line represents the contour where ϕ_{avg} equals 0.01.

behaviour observed at low turbulence intensities, between 1 % and 3 %, as shown in Fig. 9. In these cases, the fountain configurations that result in zero tracer concentration in the lower layers extend to higher values of Fr^{-2} compared to those with higher or lower turbulence intensities.

To conclude our study, Sec. III C examines the size of the region affected by the return of the fountain fluid, with the aim of predicting the real impact of the fluid that returns to the ground, beyond the average concentration detected in the lower layers of the ambient fluid.

C. Pollutant-free locations

In this section, we delve deeper into the analysis of the impact of the ejected fluid from the fountain that returns to the ground, investigating which areas are affected. For a given tracer concentration ϕ , we define the impact radius r_ϕ as fol-

lows:

$$r_\varphi(z, t) = \max \{ r \geq D, \text{ such that } \phi_{\text{avg}}(r, z, t) \geq \varphi \} \quad (4)$$

Figure 10 shows colour maps of the non-dimensional impact radius, i.e., $r_\varphi^* = r_\varphi/D$, for the same layers of ambient fluid and the same time instant chosen in the previous sections, i.e., $r_\varphi(z = 3D, t = 135\text{s})$, in the configuration space $(Fr^{-2}, u'/U)$, for two values of φ : (a) $\varphi = 0.05$ and (b) $\varphi = 0.20$. As expected, r_φ^* decreases as φ increases for each fountain configuration. Specifically, for a tracer threshold of 0.20, the ground remains unaffected for $Fr^{-2} \leq 4 \times 10^{-3}$, i.e., fountain temperatures below 10 °C, regardless of inlet turbulence intensity.

For low turbulence intensities in the range of approximately 1 % to 3 %, Fig. 10(a) shows that the lower layers of the ambient fluid remain unaffected by the return of ejected fluid over a broader range of Fr^{-2} , up to approximately 3.8×10^{-3} . For higher fluctuations, these ambient layers are unaffected by the fountain return fluid for $Fr^{-2} \geq 2.2 \times 10^{-3}$, i.e., fountain temperatures above 12.5 °C. This is in excellent agreement with the analyses in Secs. III A and III B, where we observed similar irregularities in regions of increased ambient fluid heating and lower tracer concentrations, respectively.

By defining the impact radius in this manner, we can assess the extent of the regions affected by the return of the fountain fluid for various levels of turbulence and stratification. This metric provides a practical way to quantify the influence of fountains on the ambient environment, allowing for more precise predictions of the areas impacted under different configurations.

IV. FINAL REMARKS

Here, we provided tools to predict the impact of a fountain injected into a linearly stratified environment on the lower layers of the atmosphere. The evolution of the ambient fluid exhibits distinct behaviour at low turbulence intensities. In this regime, a lower inlet temperature of the fountain, i.e., higher Fr^{-2} , hinders the increase in the average temperature of the lower ambient fluid layers. However, it simultaneously increases the protected distance from the return of ejected fluid, i.e., the impact radius is extended.

The most notable behaviour is observed in the effect on the temperature of the lower ambient layers. For $Fr^{-2} \leq 5.3 \times 10^{-3}$, i.e., injected fountain temperatures above 4 °C, the temperature of the lower ambient layers consistently increases. However, there exists an optimal region in the configuration space $(Fr^{-2}, u'/U)$, where the temperature increase is maximised. This region is independent of the fountain's turbulence intensity for $2.2 \times 10^{-3} \leq Fr^{-2} \leq 5.3 \times 10^{-3}$, except for 1 % $\leq u'/U \leq 3$ %, where the region narrows, and the temperature increase occurs for $Fr^{-2} \geq 3.8 \times 10^{-3}$, i.e., fountain temperatures below 10 °C. This behaviour can be explained based on the work of Sarasúa et al. (2024)⁴, as this region coincides with the semi-collapse regime of the fountain. In this regime, part of the fountain fluid returns to the surface but

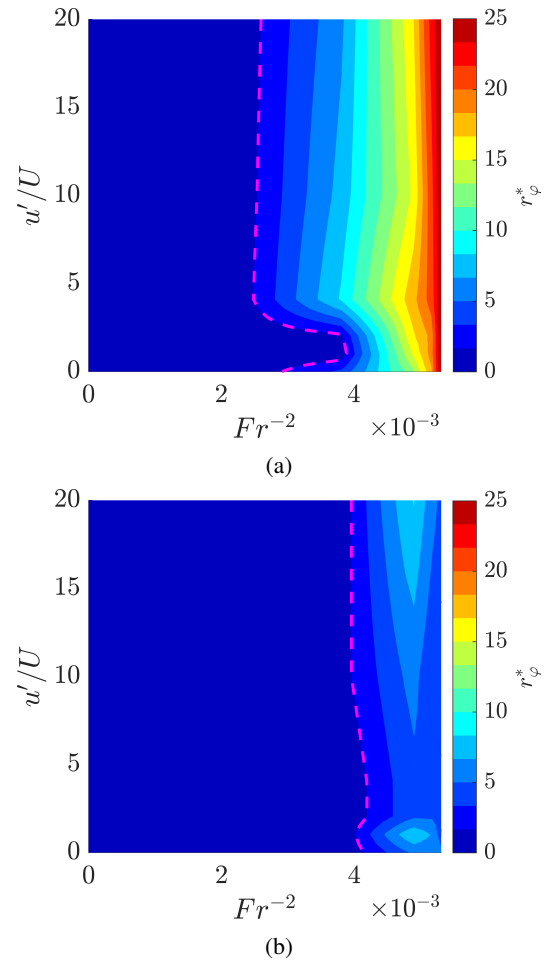


FIG. 10: Two-dimensional colour map of the radial distance r^* at which a mean tracer concentration $r_\varphi(z = 3D, t = 135\text{s})$ is detected in the lower layers of the ambient, with: (a) $\varphi = 0.05$ and (b) $\varphi = 0.20$. The magenta dashed line marks the right boundary of the configuration space free of tracer, i.e., where the concentration is below the given threshold φ .

at a lower tracer concentration, indicating that it has already mixed with ambient fluid at a higher level, i.e., at a higher temperature, which deposits this warmer fluid in the lower layers, thereby increasing the ambient temperature. The temperature evolution is thus a delicate balance between the fountain collapse regime and the characteristic heights reached by the fountain, governed by its inlet properties.

Although this model is based on conditions typically observed in the lower atmosphere during radiation frosts, the analysis is also applicable to other stratified conditions in ambient fluids. As future work, a highly interesting analysis from a technological perspective would be to study the case of injecting a plume, where T_{jet} is higher than the ambient fluid temperature at ground level. After rising to a certain height, the plume will encounter a warmer layer of fluid and will transform into a fountain. This analysis would provide insight into the potential benefits of heating the fluid ejected by the SIS device.

ACKNOWLEDGEMENTS

The authors would like to thank PEDECIBA (MEC, UdeLaR, Uruguay).

DATA AVAILABILITY

The data that support the findings of this study are available from the corresponding author upon reasonable request.

- ¹B. R. Morton, G. I. Taylor, and J. S. Turner, "Turbulent gravitational convection from maintained and instantaneous sources," *Proceedings of the Royal Society of London. Series A. Mathematical and Physical Sciences* **234**, 1–23 (1956).
- ²N. B. Kaye, "Turbulent plumes in stratified environments: A review of recent work," *ATMOSPHERE-OCEAN* **46**, 433–441 (2008).
- ³A. W. Woods, "Turbulent plumes in nature," *Annual Review of Fluid Mechanics* **42**, 391–412 (2010).
- ⁴L. G. Sarasúa, D. Freire Caporale, N. Barrere, and A. C. Martí, "The influence of source froude number and turbulent fluctuations on the development of turbulent fountains in stratified ambient," *Flow, Turbulence and Combustion* **112**, 1009–1025 (2024).
- ⁵M. Burke, L. Gusta, H. Quamme, C. Weiser, and P. H. Li, "Freezing and injury in plants," *Annual Review of Plant Physiology* **27**, 507–528 (1976).
- ⁶R. S. Pearce, "Plant freezing and damage," *Annals of botany* **87**, 417–424 (2001).
- ⁷F. P. Co., "SIS Technologies," <https://frostprotection.com/index.php?lang=en-us> (n.d.), accessed: September 25th, 2024.
- ⁸R. Guarga, P. Mastrángelo, G. Scaglione, and E. Supino, "Evaluation of the sis: a new frost protection method applied in a citrus orchard," in *Proceedings of the 9th. Congress of the International Society of Citriculture* (2000).
- ⁹M. Albertson, Y. Dai, R. A. Jensen, and H. Rouse, "Diffusion of submerged jets," *Transactions of the American Society of Civil Engineers* **115**, 639–664 (1950).
- ¹⁰M. Arias, H. Arbiza, and M. Mendina, "Two experiences of frost damage control in vineyards with selectively extraction of coldest air: Alto valle, argentina and napa valley, california, usa," in *VIII International Symposium on Temperate Zone Fruits in the Tropics and Subtropics* 872 (2007) pp. 407–414.
- ¹¹H. Yazdanpanah and C. Stigter, "Selective inverted sink efficiency for spring frost protection in almond orchards northwest of isfahan, iran," *Theoretical and Applied Climatology* **105**, 27–35 (2011).
- ¹²I. Vahid, C. Karem, T. Caroline, F. Martin, E. Rainvill, and G. Hardy, "Micrometeorological observations for the evaluation of the selective inverted sink against radiation frost and the potential of a new hybrid system," *Procedia Earth and Planetary Science* **15**, 920–927 (2015).
- ¹³Y. Hu, E. A. Asante, Y. Lu, A. Mahmood, N. A. Buttar, and S. Yuan, "Review of air disturbance technology for plant frost protection," *International Journal of Agricultural and Biological Engineering* **11**, 21–28 (2018).
- ¹⁴F. P. Co., "FPC Services," https://frostprotection.com/index.php?option=com_content&view=article&id=49&Itemid=465&lang=en-us (n.d.), accessed: September 25th, 2024.
- ¹⁵L. J. BLOOMFIELD and R. C. KERR, "Turbulent fountains in a stratified fluid," *Journal of Fluid Mechanics* **358**, 335–356 (1998).
- ¹⁶E. Kaminski, S. Tait, and G. Carazzo, "Turbulent entrainment in jets with arbitrary buoyancy," *Journal of Fluid Mechanics* **526**, 361–376 (2005).
- ¹⁷R. Mehaddi, O. Vauquelin, and F. Candelier, "Analytical solutions for turbulent boussinesq fountains in a linearly stratified environment," *Journal of Fluid Mechanics* **691**, 487–497 (2011).
- ¹⁸P. Papanicolaou and G. Stamoulis, "Spreading of buoyant jets and fountains in a calm, linearly density-stratified fluid," *Environmental hydraulics*, 123–128 (2010).
- ¹⁹M. van Reeuwijk and J. Craske, "Energy-consistent entrainment relations for jets and plumes," *Journal of Fluid Mechanics* **782**, 333–355 (2015).
- ²⁰F. P. Co., "How the Selective Inverted Sink (SIS) works in a flat and horizontal topography," https://frostprotection.com/images/2_FLATANDHORIZONTALTOPOGRAPHY.pdf (n.d.), accessed: September 25th, 2024.
- ²¹L. Sarasua, D. Freire, C. Cabeza, and A. C. Martí, "Spreading height and critical conditions for the collapse of turbulent fountains in stratified media," *Physics of Fluids* **33** (2021).
- ²²D. Freire Caporale, N. Barrere, A. C. Martí, C. Cabeza, and L. G. Sarasúa, "Elucidating coherent structures, transport barriers, and entrainment in turbulent fountains in stratified media," *Physics of Fluids* **34**, 085119 (2022).
- ²³D. Freire, C. Cabeza, S. Pauletti, G. Sarasúa, I. Bove, G. Usera, and A. C. Martí, "Effect of turbulent fluctuations on the behaviour of fountains in stratified environments," in *Journal of physics: Conference series*, Vol. 246 (IOP Publishing, 2010) p. 012015.
- ²⁴G. Usera, A. Vernet, and J. Ferré, "A parallel block-structured finite volume method for flows in complex geometry with sliding interfaces," *Flow, Turbulence and Combustion* **81**, 471–495 (2008).
- ²⁵J. H. Ferziger, M. Perić, and R. L. Street, "Finite volume methods," in *Computational Methods for Fluid Dynamics* (Springer International Publishing, Cham, 2020) pp. 81–110.